energies

MDPI

Article

Integrated Control and Optimization for Grid-Connected Photovoltaic Systems: A Model-Predictive and PSO Approach

Chaymae Boubii [1], Ismail El Kafazi [2], Rachid Bannari [1], Brahim El Bhiri [2], Saleh Mobayen [3,*], Anton Zhilenkov [4] and Badre Bossoufi [5,*]

[1] Laboratory Systems Engineering ENSA, Ibn Tofail University, Kenitra 14000, Morocco; boubii.chaymae@gmail.com (C.B.); rachid.bannari@gmail.com (R.B.)
[2] Laboratory SMARTILAB, Moroccan School Engineering Sciences, EMSI, Rabat 10150, Morocco; elkafazi.ism@gmail.com (I.E.K.); b.elbhiri@emsi.ma (B.E.B.)
[3] Graduate School of Intelligent Data Science, National Yunlin University of Science and Technology, 123 University Road, Section 3, Douliou, Yunlin 640301, Taiwan
[4] Department of Cyber-Physical Systems, St. Petersburg State Marine Technical University, 190121 Saint-Petersburg, Russia; marine_electronics@corp.smtu.ru
[5] LIMAS Laboratory, Faculty of Sciences Dhar El Mahraz, Sidi Mohamed Ben Abdellah University, Fez 30000, Morocco
* Correspondence: mobayens@yuntech.edu.tw (S.M.); badre.bossoufi@usmba.ac.ma (B.B.)

Abstract: To propel us toward a greener and more resilient future, it is imperative that we adopt renewable sources and implement innovative sustainable solutions in response to the escalating energy crisis. Thus, renewable energies have emerged as a viable solution to the global energy crisis, with photovoltaic energy being one of the prominent sources in this regard. This paper represents a significant step in the desired direction by focusing on detailed, comprehensive dynamic modeling and efficient control of photovoltaic (PV) systems as grid-connected energy sources. The ultimate goal is to enhance system reliability and ensure high power quality. The behavior of the suggested photovoltaic system is tested under varying sun radiation conditions. The PV system is complemented by a boost converter and a three-phase pulse width modulation (PWM) inverter, with MATLAB software employed for system investigation. This research paper enhances photovoltaic (PV) system performance through the integration of model-predictive control (MPC) with a high-gain DC–DC converter. It improves maximum power point tracking (MPPT) efficiency in response to the variability of solar energy by combining MPC with the traditional incremental conductance (IN-C) method. Additionally, the system incorporates a DC–AC converter for three-phase pulse width modulation, which is also controlled by predictive control technology supported by Particle Swarm Optimization (PSO) to further enhance performance. PSO was selected due to its capability to optimize complex systems and its proficiency in handling nonlinear functions and multiple variables, making it an ideal choice for improving MPC control performance. The simulation results demonstrate the system's ability to maintain stable energy production despite variations in solar irradiation levels, thus highlighting its effectiveness.

Keywords: photovoltaic system; maximum power point tracking; model predictive control; incremental conductance; particle swarm optimization

Citation: Boubii, C.; El Kafazi, I.; Bannari, R.; El Bhiri, B.; Mobayen, S.; Zhilenkov, A.; Bossoufi, B. Integrated Control and Optimization for Grid-Connected Photovoltaic Systems: A Model-Predictive and PSO Approach. *Energies* **2023**, *16*, 7390. https://doi.org/10.3390/en16217390

Academic Editor: Sandro Nizetic

Received: 1 September 2023
Revised: 19 September 2023
Accepted: 27 September 2023
Published: 1 November 2023

1. Introduction

The increasing global population and ongoing industrial advancements are fueling a substantial rise in energy demand, emphasizing the critical role of energy in our daily lives [1–3]. Historically, fossil fuels have been a cornerstone of our energy mix. However, the combination of growing energy demands, depleting fossil fuel reserves, and mounting environmental concerns has spurred a significant shift towards cleaner energy sources, including solar, hydro, and wind energy [4]. These sources offer a compelling alternative

for meeting our electricity needs while minimizing environmental impact, with solar energy emerging as a pre-eminent renewable energy source for power generation [5]. At the heart of this transition, photovoltaic (PV) systems play a pivotal role in converting solar energy into electricity [6,7]. The global PV sector has experienced substantial growth, partially attributed to the declining costs of solar modules [8]. Nevertheless, PV modules still constitute a substantial portion of the overall expenditure in a power generation system [9]. Hence, optimizing the efficiency of PV modules has become paramount in driving down electricity production costs. The construction of efficient PV systems hinges on the development of precise PV models capable of accurately predicting the output of individual PV modules, a prerequisite for tasks like optimizing PV module placement [10]. Irrespective of environmental conditions, PV solar systems employ maximum power point tracking (MPPT) methods to maximize electricity extraction. An array of MPPT algorithms, ranging from basic to sophisticated, has been devised to calculate the maximum power point (MPP) based on the application and weather conditions [11]. The primary objective of MPPT is to enhance the output power of PV modules under varying radiation and temperature conditions. Consequently, a myriad of MPPT algorithms has emerged, exhibiting varying tracking speeds, costs, and technological requirements for application and implementation [12–15]. Notably, Model Predictive Control (MPC) has surfaced as a prospective MPPT technique in PV systems, leveraging mathematical models to predict system behavior and adapt control actions accordingly [16]. The core contribution of this study lies in the prediction of a single-step temporal horizon error using the MPC framework to amplify energy harvesting efficiency within the well-established incremental conductance (IN-C) MPPT method. While IN-C excels in energy harvesting, its control eventually converges to a limit cycle centered around the MPP, constraining its ability to quantify transient solar irradiance due to its relatively slow operation [17]. The proposed method strives to enhance the energy capture capability of PV panels. The PV system integrates with the power grid via a DC–DC chopper and a DC–AC inverter, with numerous strategies proposed for optimizing this integration. One such approach involves controlling the DC–DC chopper through an MPPT technique, ensuring optimal energy extraction even under fluctuating environmental conditions [18–21]. Significantly, considerable attention has been devoted to control schemes for DC–AC inverters to bolster the operational performance of grid-connected PV systems during unforeseen circumstances. These control systems facilitate active and reactive load flow management between the grid and the PV system, playing a pivotal role in enhancing system stability and improving voltage profiles at the Point of Common Coupling [22–25]. Previous studies have advocated for the use of PI controllers to enhance transient stability in grid-connected PV systems [26]. However, conventional PI control has proven insufficient in achieving significant system stability enhancements. To address this limitation, this study introduces a novel control scheme designed to deliver prompt responses, reliable dynamic performance, and mitigation of adverse effects on the inverter or degradation in power quality [27,28]. One notable advantage of utilizing MPC is its capacity to streamline the development of various controllers while accommodating system constraints within its formulation. Moreover, this work recommends the incorporation of Particle Swarm Optimization (PSO) as a user-friendly optimization technique to augment the cost function of the MPC controller. The subsequent sections of this document are structured as follows: Section 2 provides an overview of the PV system's components and their respective roles, along with the proposed control mechanism based on PSO optimization and predictive control. In Section 3, we elaborate on the simulation methodology and present the obtained results. Finally, Section 4 concludes the manuscript, underscores its contributions, and suggests avenues for future research.

2. Configuration of PV System

The proposed PV system in this study is divided into many components. First, solar energy is transformed into electrical energy using a solar panel. The array's output voltage is then raised while still preserving the desired voltage level by using a boost converter.

To convert the DC to AC while maintaining a power factor of one, a DC–AC converter is supplied. A transformer is also used to increase the output voltage to the required level for a common connection. The control group of the system consists of many techniques that have been researched to improve power extraction, keep a power factor of one, and alter junction voltage [29,30]. Figure 1 shows the photovoltaic system's complete configuration.

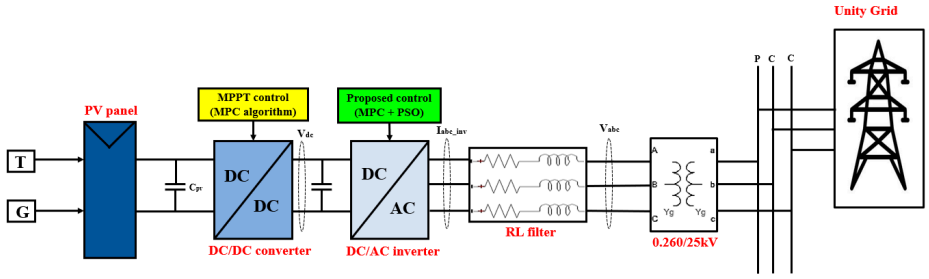

Figure 1. The PV system.

The modeling of a solar power system and its performance are the main topics of this section. It starts off by outlining the PV module's features. It discusses how the PV module responds to changes in temperature and sun irradiation. Also incorporated is the boost converter, which oversees the decrease in the PV array's output voltage. The boost converter's operation and its control methods, including the MPPT methodology, are thoroughly detailed. Regardless of the shifting external circumstances, the PV system always functions at its maximum power production thanks to the MPPT technology. The section also discusses the DC–AC inverter, which transforms DC electricity produced by a PV array into AC power for grid integration. A power factor of one is maintained while discussing the operation and control of the DC–AC converter. Overall, the PV module, boost converter, MPPT approach, and DC–AC inverter are all covered in-depth in this section's discussion of the modeling, performance, and control aspects of the PV system.

2.1. Photocell Panel

In the literature, various models have been presented to characterize photovoltaic panels, demonstrating a range of designs. For instance, Rauschenbach (1980) [31] employed a single-diode model, while Barth et al. (2016) [32] proposed a two-diode model that accounts for carrier recombination effects. In addition, Nishioka et al. (2007) [33] utilized a three-diode model to capture additional effects disregarded by the two-diode model. The common objective of these models is to optimize energy extraction from the panels, considering the influence of solar radiation and temperature [34,35]. The single-diode type has become the most well-liked of these due to its improved accuracy and simplicity [36].

The single-diode model shown in Figure 1 includes resistive losses that are accounted for by series and shunt resistances, an anti-parallel diode that characterizes the non-linear impedance of the P-N junction, and a photogenerated current component that is affected by temperature and radiation [37]. Equations (1)–(5) encapsulate the mathematical formulation of the photovoltaic panel [38–40].

$$I = N_p \,.\, I_{ph} - N_p \,.\, I_{rs} \,.\, e^{\left(\frac{V + R_s \,.\, I}{A \,.\, V_t \,.\, N_s} - 1\right)} - I_{sh} \tag{1}$$

$$I_{ph} = (I_{scn} + k_i \,.\, (T - T_n)) \,.\, \frac{G}{1000} \tag{2}$$

$$I_{rs} = I_{rs0} \,.\, \left(\frac{T_n}{T}\right)^3 \,.\, e^{\left(\left(\frac{q \,.\, E_g}{k \,.\, A}\right) .\, \left(\frac{1}{T_r} - \frac{1}{T}\right)\right)} \tag{3}$$

$$V_t = \frac{k \,.\, T}{q} \tag{4}$$

$$I_{sh} = \frac{V_{pv} + R_s \,.\, I_{pv}}{R_{sh}} \tag{5}$$

where:

- I: Current output of a PV generator.
- I_{rs}: Temperature-dependent diode saturation current expressed.
- I_{ph}: photon current in a PV cell.
- I_{sh}: Shunt current.
- I_{scn}: short circuit current at ($T_r = 25$ °C and $G_n = \frac{1000W}{m^2}$) for PV cells.
- k_i: Coefficient of the current I_{scn} in A/K. k: Boltzmann's constant.
- q: Electron charge constant.
- A: Ideality factor is another name for the diode quality factor.
- V_t: Thermodynamic potential (also called thermal tension).
- N_p: Number of parallel PV modules.
- N_s: Number of PV cells in series.
- I_{rs0}: Rated diode saturation current (at $T_r = 25$ °C).
- E_g: Energy gap of the polycrystalline SI (eV).
- R_s: Series Resistance of a PV module.
- R_{sh}: Shunt Resistance of a PV module.

The PV system's specifications are listed in Table 1. Figure 2 depicts the I-V and PV characteristics of the PV array under various sun irradiation intensity situations because of modeling.

Table 1. Specifications of solar panel.

Parameter	Specification
Series-connected modules per string	10
Parallel string	40
Module	1Soltech 1STH-215P
Maximum power	213.5
Voltage at maximum power point	29
Current at maximum power point	7.35
Short circuit current	7.84
Open circuit voltage	36.3

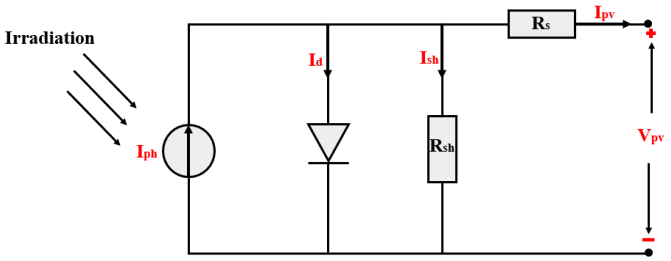

Figure 2. The single-diode model of PV panel.

The Figure 3 presents the PV panel characteristic, I-V and P-V.

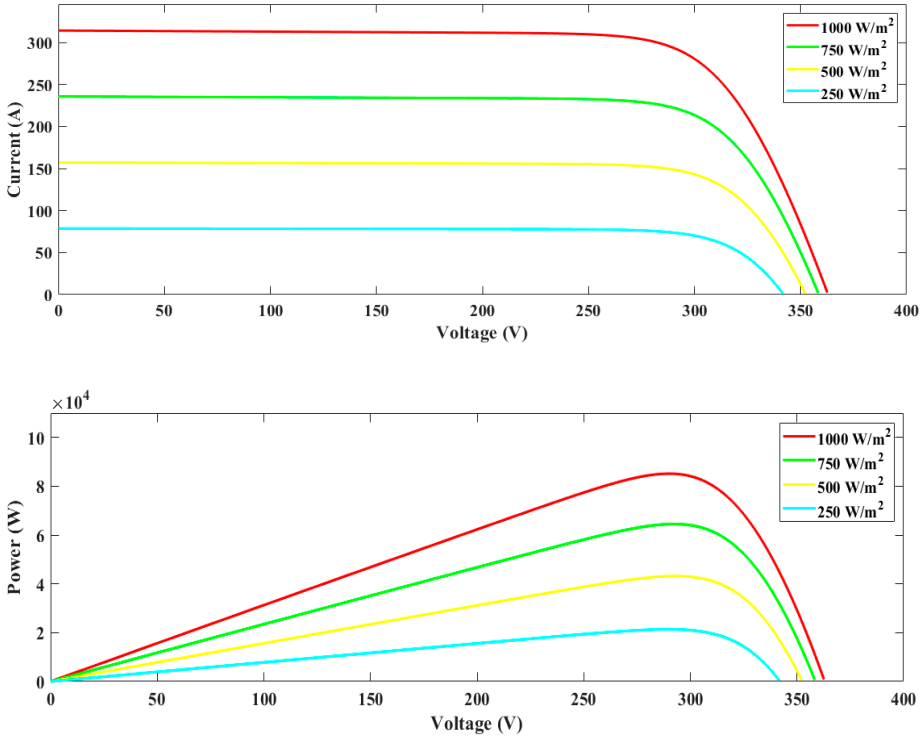

Figure 3. Solar Cell I-V and P-V Curves at Various Irradiances.

2.2. Boost Converter for DC-DC

Using a boost converter in this situation aims to increase the input voltage until it reaches the desired output voltage without using a transformer [41]. As seen in Figure 4, an inductor, a capacitor, a diode, and a high-frequency switch are the essential parts of a boost converter. The equations mentioned below [42] are a result of the high-frequency switch's operational state:

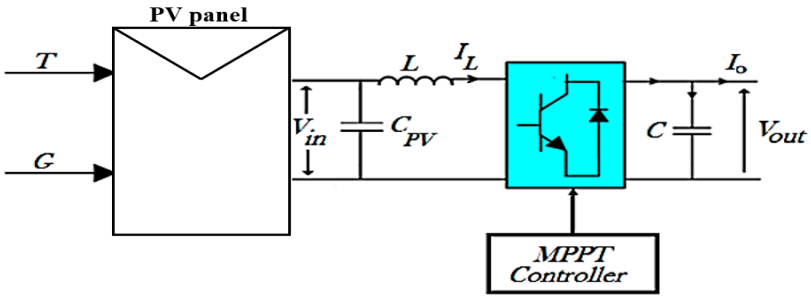

Figure 4. PV panel with Boost converter.

For S in mode on:

$$L \cdot \frac{di_{Lb}(t)}{dt} = v(t) \tag{6}$$

When S in mode off:

$$L \cdot \frac{di_{Lb}(t)}{dt} = v(t) - v_{Cb}(t) \tag{7}$$

If S = 1 and S = 0, the conversion is between ON and OFF.
The duty ratio is

$$D = 1 - \frac{v(t)}{v_{Cb}(t)} \tag{8}$$

Consequently,

$$v_{Cb}(t) = \frac{1}{1-D} \,.\, v(t) \tag{9}$$

where,

v: the PV system's electrical potential, also known as PV voltage, serves as both the output from the PV array and the input voltage to a DC–DC converter.

v_{Cb}: the boost converter's capacitance voltage and the intended boost converter output voltage.

$i_{Lb}(t)$: the inductance current to boost converter.

L: boost inductance.

2.3. MPPT MPC

Since the 1980s, MPC has been used in power electronics for low-switching-frequency, high-power applications [43,44]. At the time, widespread implementation of the MPC method was not possible due to the high switching frequencies that demanded quick processing. Thanks to developments in high-speed microprocessors, interest in the use of MPC for power converters with higher switching frequencies has grown during the past ten years [45–47]. The main purpose of MPC is to predict how the control variables will behave up until a specific time [44]. Using the anticipated control variables, the best switching state can be discovered by minimizing a cost function. For prediction, the control variables' discrete time model and state space model are employed [44].

$$x(k+1) = A \,.\, x(k) + B \,.\, u(k) \tag{10}$$

$$y(k) = C \,.\, u(k) \tag{11}$$

Consequently, one can define a cost function as follows that considers future actuations, references, and states:

$$j = g(x(k),\ u(k),\ \ldots, u(k+N-1)) \tag{12}$$

The defined cost function g considers future states, references, and actuation. On the time horizon N, this cost function ought to be reduced for a certain step. When only the first element of the sequence is applied by the controller, the output $u(k)$ will be a sequence of N optimum actuations:

$$u(k) = [1\ 0 \ldots 0] argmin_u\ j \tag{13}$$

The proposed MPPT algorithm is displayed in Figure 5. The algorithm considers the entrance tension and current of the PV system, and the voltage that is produced when the switch is turned on and off using (6) and (7).

$$c \,.\, \frac{dv(t)}{dt} = i(t) - i_{Lb}(t) \tag{14}$$

The discharges in (6), (7), and (14) may be approximated using the direct Euler approach:

$$\frac{dx(t)}{dt} = \frac{X(k+1) - X(k)}{T_S} \tag{15}$$

where k is the discretized time, x is the discretization parameter, and Ts is the sampling time.

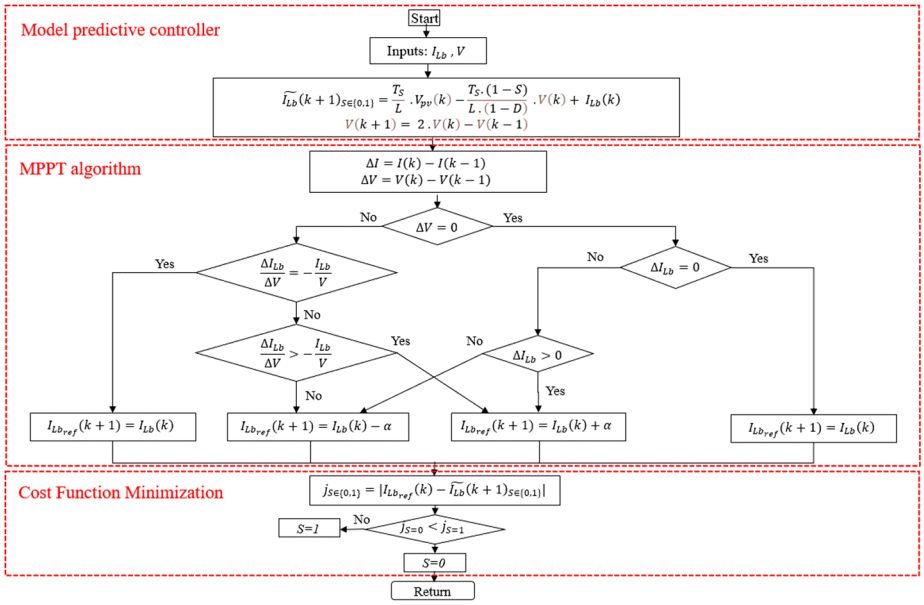

Figure 5. The proposed algorithm for MPPT controller using MPC method.

The controlled variable acts because of the process of constructing discrete time equations. Future time points k can be predicted by the control. With S in the ON (S = 1) mode, (16)–(19) for (6), (7), (14) and (15) result in the discrete-time model of the transducer:

$$I_{Lb}(k+1) = \frac{T_S}{L} \,.\, V(k) + I_{Lb}(k) \tag{16}$$

$$V(k+1) = \frac{T_S}{c} .(\, I(k) - I_{Lb}(k)) + V(k) \tag{17}$$

And if S is equal to 0, then

$$I_{Lb}(k+1) = \frac{T_S}{L} \,.\, (V(k) - V_{c2}(k)) + I_{Lb}(k) \tag{18}$$

$$V(k+1) = \frac{T_S}{c} .(\, I(k) - I_{Lb}(k)) + V(k) \tag{19}$$

From (16) to (19) there are four entries: I, I_{Lb}, V, and V_c. These equations can be adjusted to require fewer detectors by lowering the number of entry tags. With the aid of (9), V_c may be taken out of (18), so for S = 0:

$$I_{Lb}(k+1) = \frac{T_S}{L} \,.\, V(k) - \frac{T_S}{L \,.\, (1-D)} \,.\, V(k) + I_{Lb}(k) \tag{20}$$

Euler's backward technique is applied in [48] and (14):

$$V(k) - V(k-1) = \frac{T_S}{c} .(\, I(k) - I_{Lb}(k)) \tag{21}$$

Having obtained Equations (17), (19), and (21), they can be represented as follows:

$$V(k+1) = 2 \,.\, V(k) - V(k-1) \tag{22}$$

Therefore, I_{pv} is eliminated from (12) and (14).

The system configuration when the interrupter is ON and OFF is represented by the matrices (18) and (19), respectively.

When $S = 1$, it indicates that the interrupter is in the ON state.

$$\begin{bmatrix} I_{Lb}(k+1) \\ V(k+1) \end{bmatrix} = \begin{bmatrix} 1 & \frac{T_S}{L} \\ 0 & 2 \end{bmatrix} \cdot \begin{bmatrix} I_{Lb}(k) \\ V(k) \end{bmatrix} + \begin{bmatrix} 0 \\ -1 \end{bmatrix} . V(k-1) \tag{23}$$

Conversely, when $S = 0$, it signifies that the interrupter is in the OFF state.

$$\begin{bmatrix} I_{Lb}(k+1) \\ V(k+1) \end{bmatrix} = \begin{bmatrix} 1 & \frac{T_S}{L} - \frac{T_S}{L\,.\,(1-D)} \\ 0 & 2 \end{bmatrix} \cdot \begin{bmatrix} I_{Lb}(k) \\ V(k) \end{bmatrix} + \begin{bmatrix} 0 \\ -1 \end{bmatrix} . V(k-1) \tag{24}$$

The two matrices (23) and (24) were then incorporated in Figure 5 using the two-input algorithms $I_{Lb}(k)$ and $V(k)$. Figure 5 illustrates how the switch's state connects the current $I_{Lb}(k+1)$ to the future state. S can have a value of either 1 or 0. Consequently, to calculate the value of I_L in the future, a small offset value is either added or subtracted "α" from $I_{Lb}(k)$ to obtain $I_{Lb_{ref}}(k+1)$. $I_{Lb_{ref}}(k+1)$ in Figure 5 equals $I_{Lb}(k)$ when

$$\frac{dP}{dV} = 0 \tag{25}$$

by using (25)

$$\frac{d(i_{Lb}\,.v)}{dv} = 0 \tag{26}$$

from (26)

$$\frac{(i_{Lb}\,.\,d(v) + v\,.\,d(i_{Lb})}{dv} = 0 \tag{27}$$

using (27)

$$i_{Lb} + \frac{v\,.\,\partial(i_{Lb})}{\partial v} = 0 \tag{28}$$

Equation (28) must be satisfied for (29) to determine (30), consequently

$$I_{Lb_{ref}}(k+1) = I_{Lb}(k) \tag{29}$$

$$\frac{\Delta i_{Lb}}{\Delta v} = -\frac{i_{Lb}(k)}{v(k)} \tag{30}$$

In state, the program determines Δv, and Δi_{Lb} to avoid the singularity in (30). Figure 5 shows the specifics. At the sampling instant, the reference $I_{Lb_{ref}}(k+1)$ is the current to follow and serves as the input for the minimized cost function. The cost function's subject minimization is provided by

$$j_{S\in\{0,1\}} = \left| I_{Lb_{ref}}(k) - \tilde{I}_{Lb}(k+1)_{S\in\{0,1\}} \right| \tag{31}$$

After minimization, the cost function is represented by Equation (31). Figure 5 depicts the overall controller flow in its entirety.

2.4. DC/AC Inverter Controller

In this study, the photovoltaic system is connected to the utility infrastructure by a three-phase DC–AC voltage source inverter (VSI). The two-level, three-phase VSI that was selected for investigation is shown in Figure 6. The energy conversion process is enabled by the gate signals a, a′, b, b′, c, and c′, which are managed by the six power semiconductor switches (S1–S6) in this VSI architecture.

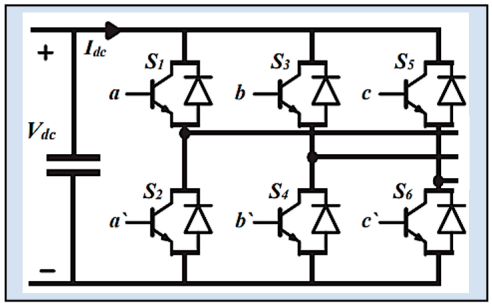

Figure 6. DC–AC inverter.

The DC–AC voltage source inverter (VSI) plays a pivotal role in grid-connected PV systems by governing energy conversion and power injection into the utility grid. This study focuses on VSI control to achieve specific objectives: correcting the power factor to nearly unity, effectively managing active power flow to the utility grid, and regulating the DC-bus voltage. A comprehensive controller, illustrated in Figure 7, has been developed to facilitate these control objectives.

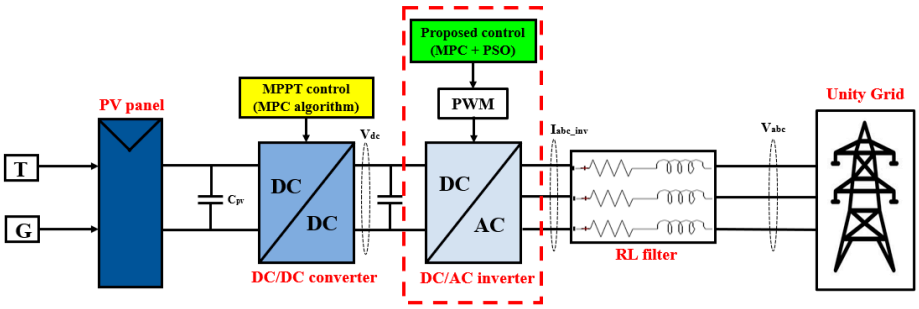

Figure 7. DC–AC Inverter controlled by MPC&PSO.

The controller comprises an external voltage control loop for precise voltage regulation and an internal current control loop for accurate current regulation. This integrated control system enables the PV system to operate at its optimal and most stable level when connected to the grid.

Figure 7 depicts the schematic representation of the inverter control scheme proposed in this study. The primary goals of this scheme include DC-link voltage regulation, precise control of real power injection, and achieving a unity power factor at the Point of Common Coupling (PCC). This control approach stands out due to its capacity for decoupled control and its rapid dynamic response, as documented in reference [49].

A. MPC controller

This paper introduces a proposed DC–AC inverter control unit that utilizes the MPC method. The design of the MPC controller is based on Equations (32) and (33) as presented in the study.

$$v_{d_{inv}} = v_d + R.i_d + L.\frac{di_d}{dt} - \omega.L.i_q \tag{32}$$

$$v_{q_{inv}} = v_q + R.i_q + L.\frac{di_q}{dt} + \omega.L.i_d \tag{33}$$

The two Equations (32) and (33) become

$$\frac{di_d}{dt} = \frac{1}{L}.\left(v_{d_{inv}} - v_d\right) - \frac{R}{L}.i_d + \omega.i_q \tag{34}$$

$$\frac{di_q}{dt} = \frac{1}{L}.(v_{q_{inv}} - v_q) - \frac{R}{L}.i_q - \omega.i_d \tag{35}$$

When using the MPC method on Equations (34) and (35), their equations become

$$I_d(1+k) = I_d(k) + \frac{T_s}{L}.(V_{d_{inv}}(k) - V_d(k)) - \frac{R\,.\,T_s}{L}.I_d(k) + \omega.T_s.I_q(k) \tag{36}$$

$$I_q(1+k) = I_q(k) + \frac{T_s}{L}.(V_{q_{inv}}(k) - V_q(k)) - \frac{R\,.\,T_s}{L}.I_q(k) - \omega.T_s.I_d(k) \tag{37}$$

The cost function proposed by this paper is

$$j = \left(I_{d_{ref}}(k) - I_d(1+k)\right)^2 + \left(I_{q_{ref}}(k) - I_q(1+k)\right)^2 \tag{38}$$

B. MPC controller optimizing with PSO

Kennedy and Eberhart [50] proposed the PSO algorithm, an evolutionary method that makes use of swarm intelligence. It shows that, even with fewer iterations, it is possible to efficiently optimize extreme points and find global minima inside the search space. The PSO algorithm is resilient to the particle's initial position and can locate both local and global optima within a given range. Due to its adaptability, it can be used to solve a variety of optimization issues, including MPC. The main goal of MPC is to minimize a certain objective function over a finite time horizon while taking system dynamics and limitations into account. Different control goals, such as limiting tracking error, cutting energy use, or cost optimization, can be represented by the objective function. By simulating a set of particles, PSO in the context of MPC optimizes control inputs across the prediction horizon. Within the search space, each particle represents a voltage reference solution [51]. The particles consider their own best location, known as the local best, and travel in the direction of the global best voltage reference that the swarm has discovered. Particle locations and velocities, which are adjusted throughout each algorithm iteration depending on the assessment of their fitness function, control how they travel (Figure 8).

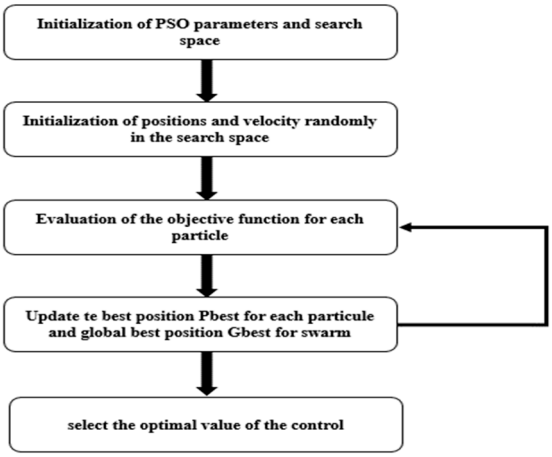

Figure 8. The flow chart of PSO.

The MPC-PSO control method optimizes an objective function comprising two distinct components: current *Id* and current *Iq*. Additionally, the objective function is computed over a specific period using the predicted DC–AC current results. The Particle Swarm Optimization (PSO) algorithm is employed to solve this optimization problem.

The particles' movement is directed towards the particle that possesses the best global position. These equations govern their direction:

$$V_{dinv\ i}(j+1) = V_i(j+1) + V_{dinv\ i}(j) \tag{39}$$

$$V_{dinv\ i}(j+1) = m_i\ .V_i(j) + c_1.r_1.\left(V_{dinv\ i}{}^{b}(j) - V_{dinv\ i}(j)\right) + c_2.r_2.\left(V_{dinv\ i}{}^{Gb}(j) - V_{dinv\ i}(j)\right) \tag{40}$$

$$V_{qinv\ i}(j+1) = V_i(j+1) + V_{qinv\ i}(j) \tag{41}$$

$$V_{qinv\ i}(j+1) = m_i\ .V_i(j) + c_1.r_1.\left(V_{qinv\ i}{}^{b}(j) - V_{qinv\ i}(j)\right) + c_2.r_2.\left(V_{qinv\ i}{}^{Gb}(j) - V_{qinv\ i}(j)\right) \tag{42}$$

where

- $V_i(j+1)$: The direction of movement of voltage in iteration $j+1$;
- m_i: Inertia weight;
- c_1, c_2: Cognitive and social acceleration coefficient;
- r_1, r_2: The random number between 0 and 1;
- $V_i{}^{b}(j)$: The personal best value of voltage for particle i for *dinv* and *qinv*;
- Gb: The global best value of voltage for the swarm for *dinv* and *qinv*;
- $V_i(j)$: The value of voltage for each particle i at iteration j for *dinv* and *qinv*.

3. Simulation and Results

In this part, the system's performance was evaluated at various levels of solar irradiation while keeping the temperature of the PV array constant at 25 °C. Standard test conditions (STC) were used to measure the solar panels' output at a temperature of 25 °C. Figure 9 shows how the sun's irradiance varies and how the pattern of irradiation changes throughout the day.

A. Simulation

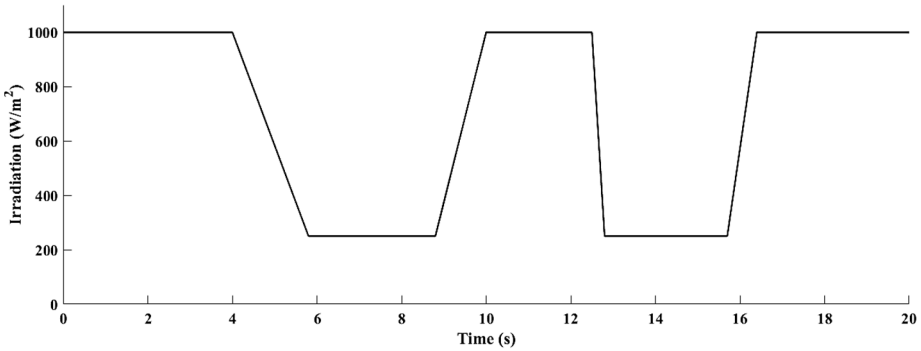

Figure 9. The variation in irradiation with temperature fixed at 25 °C.

The PV system's Simulink model, which depicts the interconnected parts and their interactions, is shown in Figure 10. The PV module, boost converter, MPPT algorithm, DC–AC inverter, and other important components are all simulated by different blocks that make up the model. The solar panel is represented by the PV module block, which also incorporates the mathematical model used to describe its electrical properties. It creates the corresponding current–voltage (I-V) and power–voltage (P-V) curves by considering the input solar irradiance and temperature. The boost converter block oversees the decrease in the PV array's output voltage. It contains the control algorithm used to govern the operation of the boost converter using the MPPT technique. For maximum power extraction, the MPPT algorithm continuously monitors and modifies the PV system's operating point. The DC–AC inverter block transforms the DC power produced by the PV array into grid-compatible AC electricity. The quality and compatibility of the generated AC power with

the utility grid are maintained, and a power factor of one is guaranteed. Transformers and grid connections are examples of additional model building pieces that might be used to represent the entire PV system and its link to the electrical grid. The Simulink model in Figure 10 offers a thorough description of the PV system overall, allowing simulation and study of its performance under various operating conditions and control schemes.

B. Results

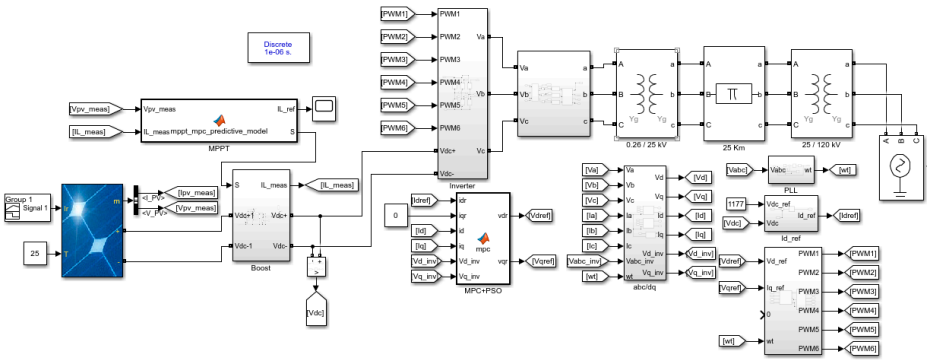

Figure 10. Simulation of PV system in MATLAB/Simulink.

As shown in Figure 11, the proposed PV system can be separated into three major components, designated as A, B, and C. These three components serve different purposes to ensure the effective generation, conversion, and integration of solar energy into the electrical grid, respecitvely. They each represent various elements or stages within the system.

C. Part A: PV System

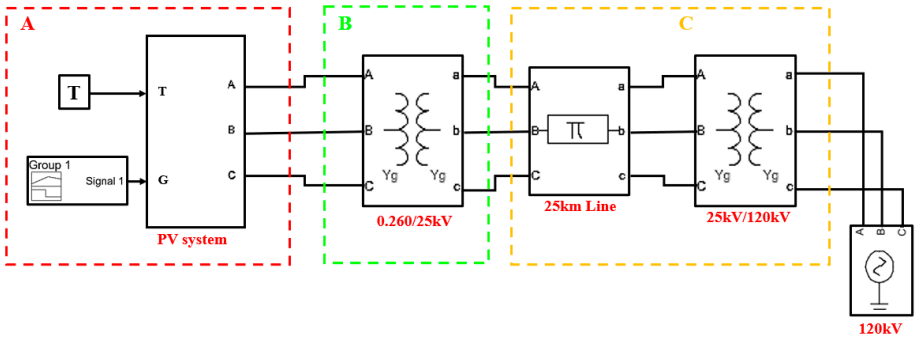

Figure 11. The overall diagram of the proposed PV system.

This segment represents the fundamental elements of the PV system. It all starts with the PV panel, which is responsible for converting solar radiation into electrical energy. Additionally, the system employs a boost converter and MPPT control with the MPC method. The main purpose of the boost converter is to raise the output voltage of the PV array, which improves the efficiency of the power conversion process. The MPPT control algorithm continually tracks and monitors the maximum power point of the PV system. By constantly adjusting the boost converter's operational parameters, it ensures that the PV panel harvests the optimal amount of power under varying climatic circumstances. The system also includes a DC–AC converter, which converts the DC power generated by the PV system into AC power suitable for grid integration. This converter must maintain a power factor of one, guarantee effective power transmission, and adhere to grid connection rules to enable the smooth integration of renewable energy into the existing power system.

For reference, Figure 12 displays the voltage profile of the solar panel utilized in the recommended system. The graph shows how the voltage changes over time and offers valuable details on the characteristics and actions of the PV panel. This information is necessary to comprehend the PV panel's efficiency and output in producing power.

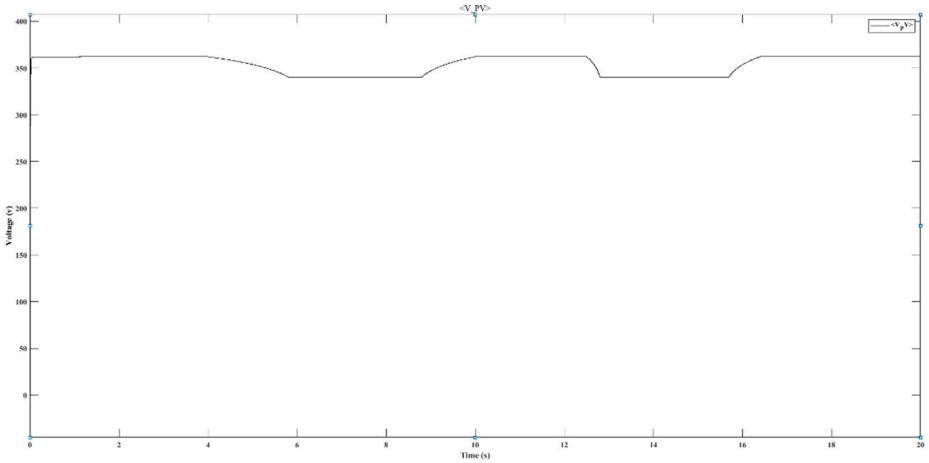

Figure 12. PV voltage.

Figure 13 displays the output voltage profile of the boost converter for the PV system. This graph shows the voltage behavior over time and demonstrates how effectively the boost converter regulates and reduces the PV panel voltage. The recorded voltage values give crucial details regarding the converter's efficiency, stability, and adaptability to changing environmental conditions. Figure 14 displays the sinusoidal waveforms of the three-phase injected current. Figure 15 shows how much actual power the system's part A generates. The characteristics of the generated voltage and current are finally displayed in Figure 16. These facts offer a full understanding of the electrical characteristics and functionality of the PV system.

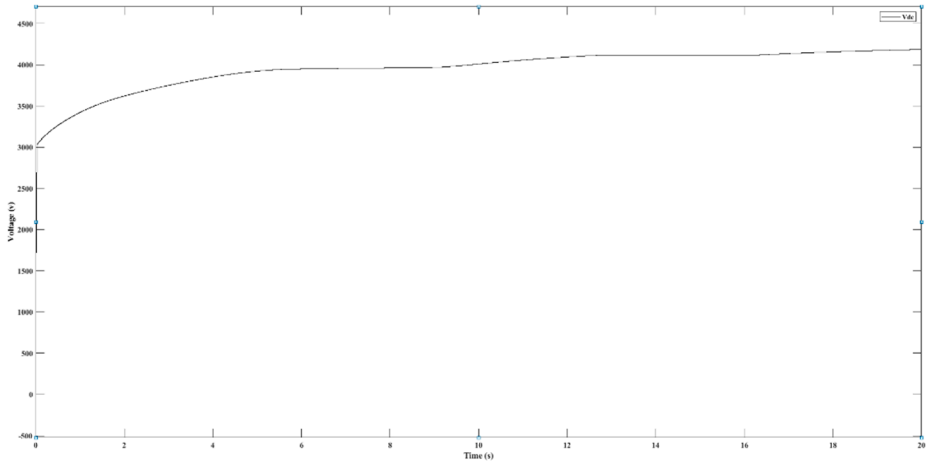

Figure 13. Boost voltage.

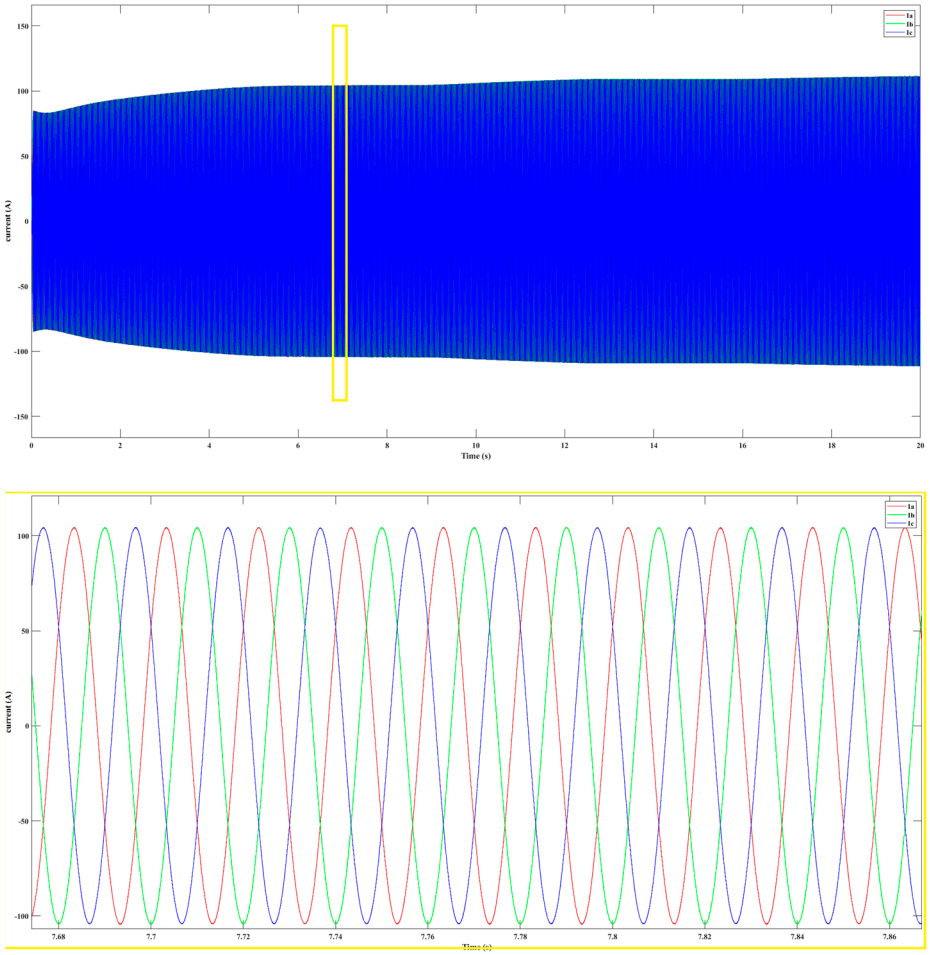

Figure 14. Current produced by part A.

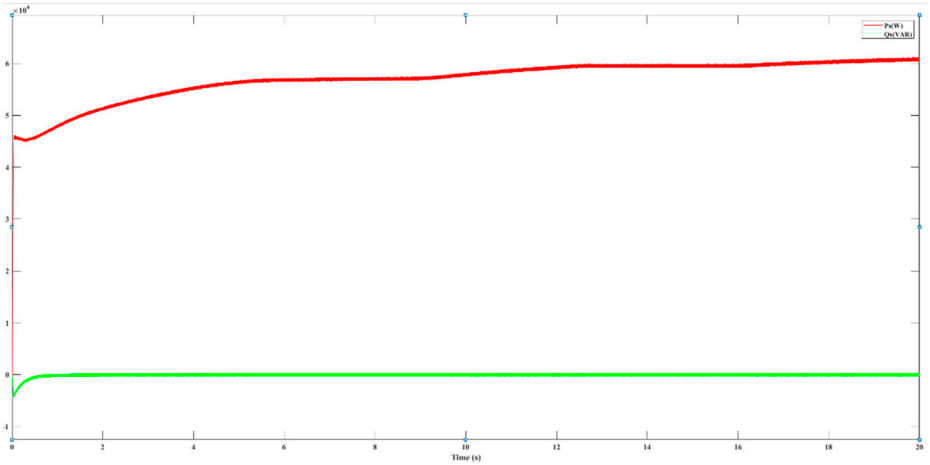

Figure 15. Active and reactive powers produced by part A.

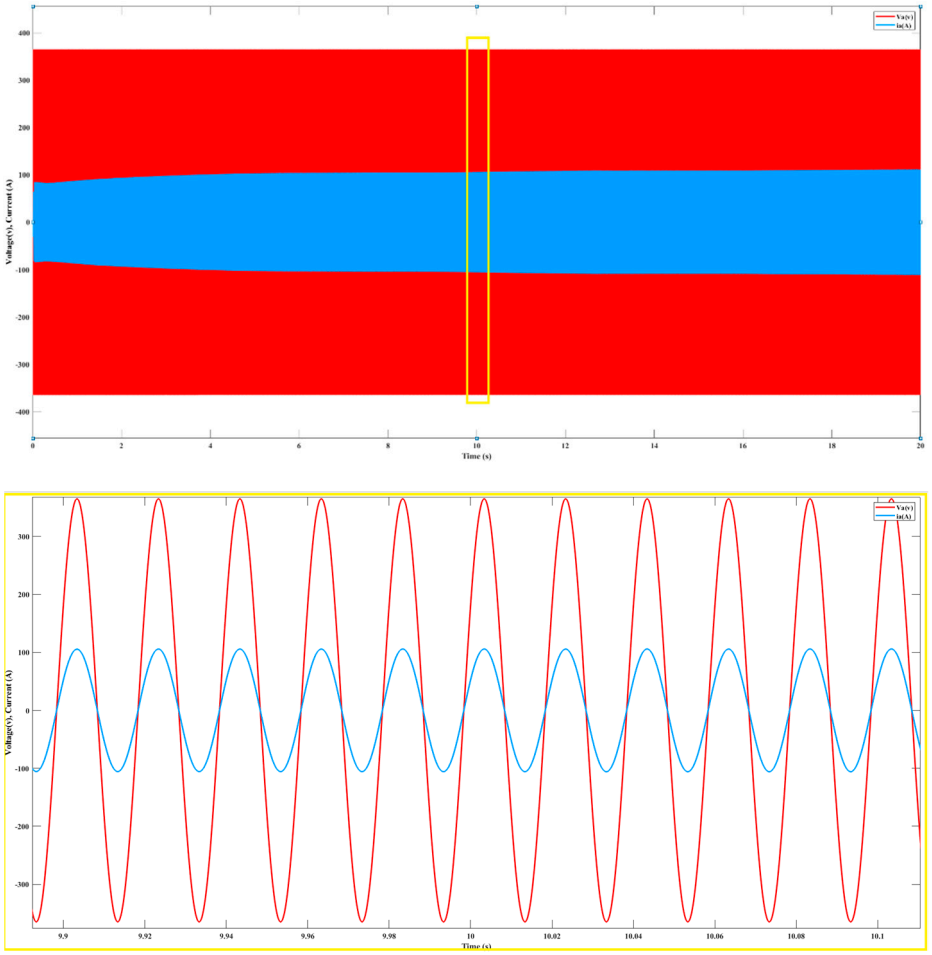

Figure 16. Current and voltage produced by part A.

➢ **Part B: Transofrmer**

The transformer's main function in component B of the PV system is to boost the system's voltage. This is necessary to ensure that the power grid's voltage requirements are met, enabling effective power transmission. Power losses during the transmission process can be reduced by lowering the current by raising the voltage level. Additionally, increasing the voltage makes it possible to transmit electrical energy farther away with fewer losses. Figures 17–19 show the outcomes of the PV system's performance with the addition of a transformer with a 0.26/25 kV rating.

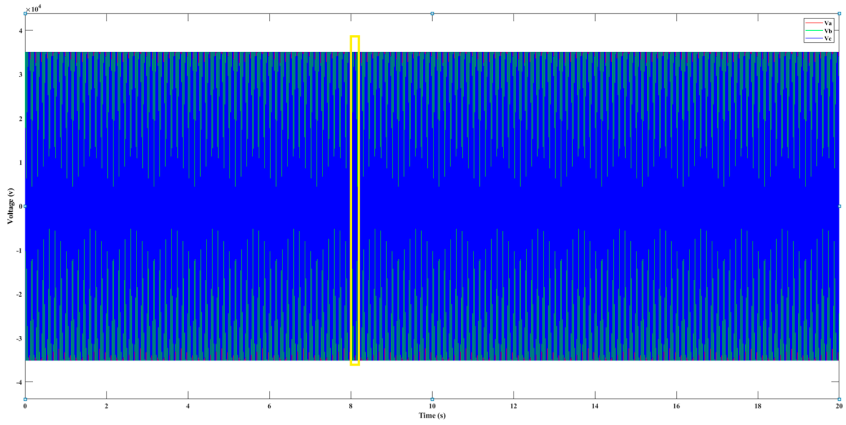

Figure 17. *Cont.*

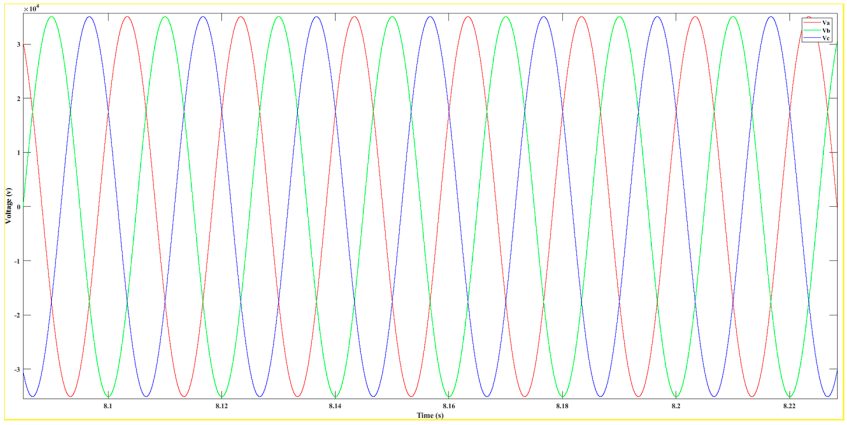

Figure 17. Voltage produced after the transformer 0.26/25 kV.

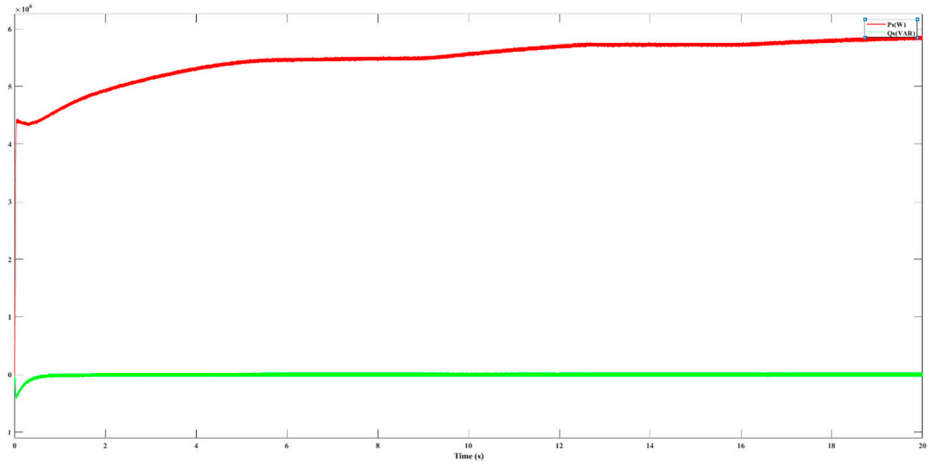

Figure 18. Active and reactive powers produced after the transformer 0.26/25 kV.

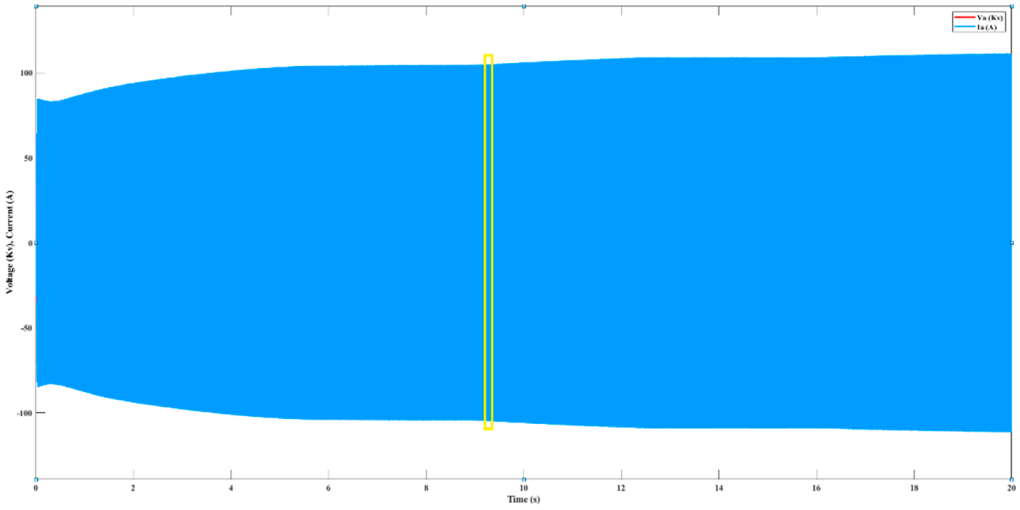

Figure 19. *Cont.*

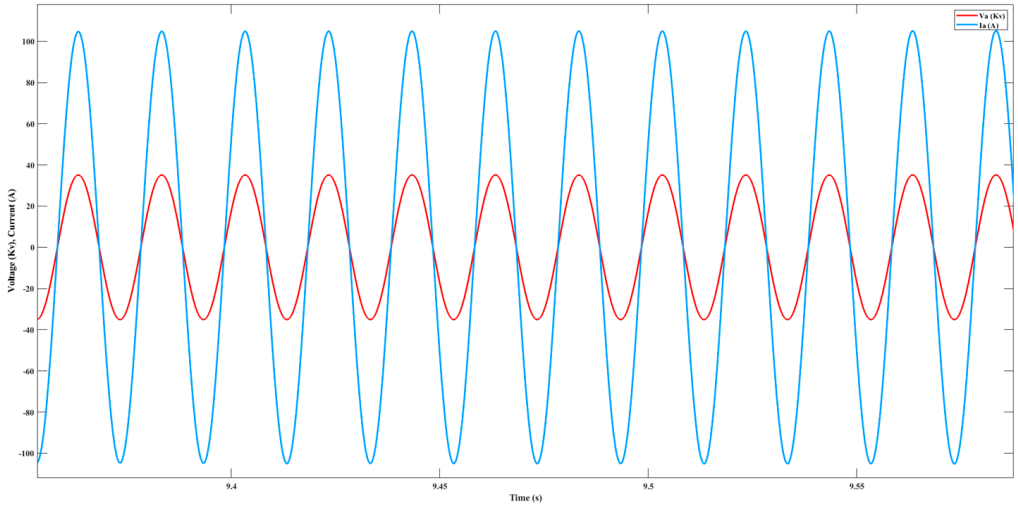

Figure 19. Current and voltage produced after the transformer 0.26/25 kV.

➢ **Part C: Transmission line, Transformer and Load**

The PV system's Part C comprises two blocks. The first block represents a 25 km transmission line, which is used to connect the PV system's electrical grid with the outside world. The second block is a transformer that oversees the increase in voltage of the power before it enters the electrical grid. To successfully transfer the generated electricity to the intended destination, which is the electrical grid, a significant distance must be covered by the 25 km transmission line. By reducing losses and voltage drops along its route, this transmission line is essential in preserving the stability and effectiveness of power transmission. On the other side, the transformer in part C's function is to raise the power's voltage to the needed levels for the electrical grid infrastructure. To maintain effective electrical distribution and transmission inside the system, this voltage step-up is required. Figures 20–22 show the results of the PV system after the 25 km transmission line and voltage step-up transformer were put into place in section C.

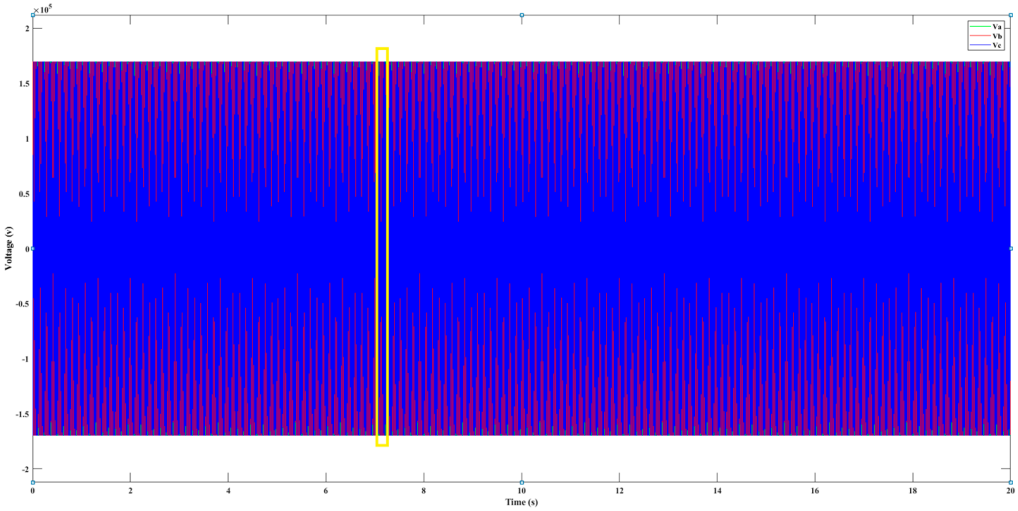

Figure 20. *Cont.*

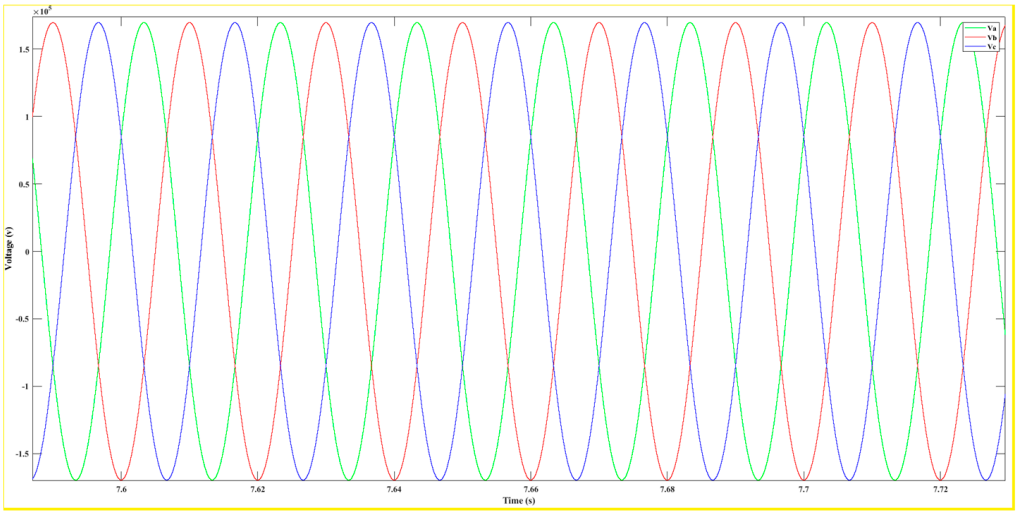

Figure 20. Voltage produced after the transformer 25/120 kV.

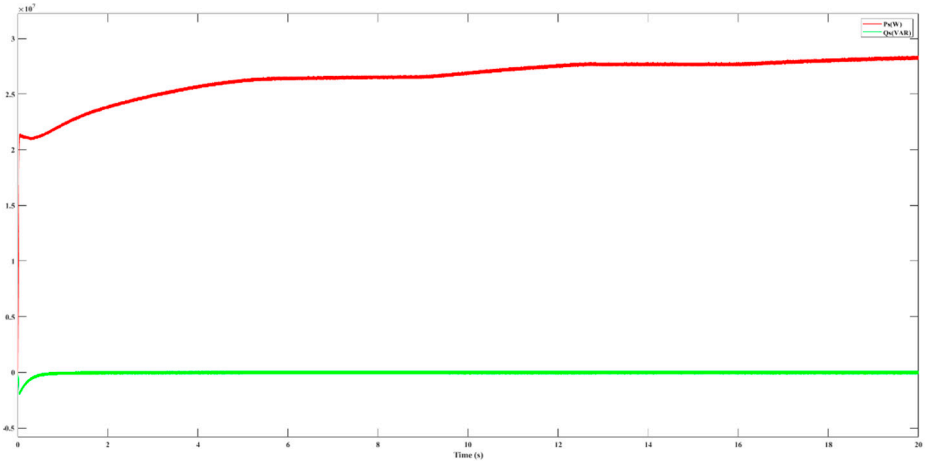

Figure 21. Active and reactive powers produced after the transformer 25/120 kV.

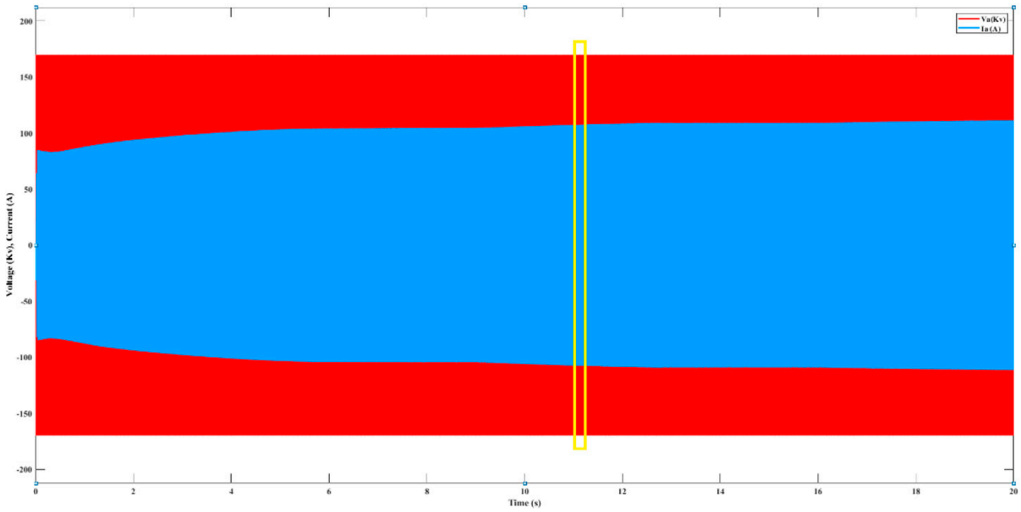

Figure 22. *Cont*.

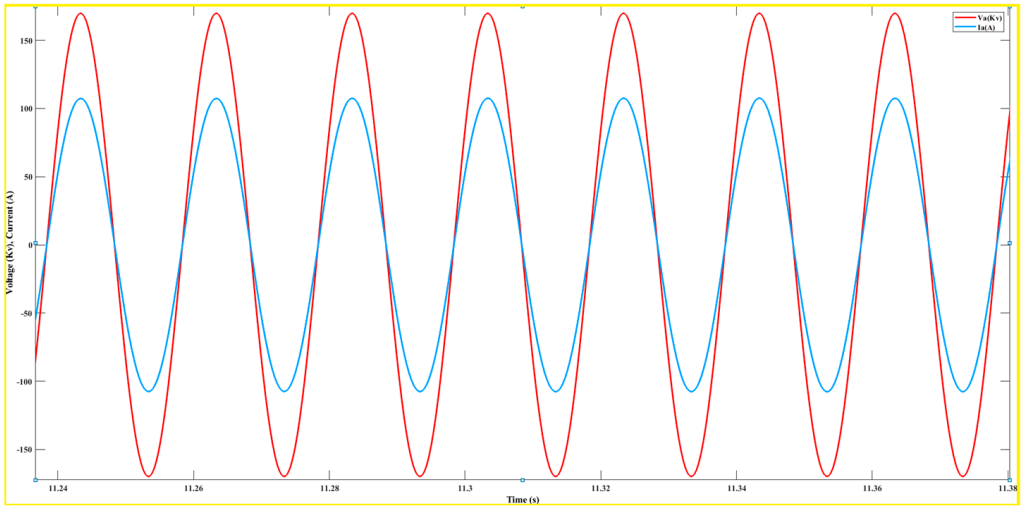

Figure 22. Current and voltage produced after the transformer 25/120 kV.

C. Discuss and compare results

In this investigation, the controllers employed, based on mathematical principles, yielded promising outcomes. Despite fluctuations in solar radiation throughout the day, the total energy output has demonstrated a remarkable degree of consistency, resulting in a steady supply of 27 MW of pumped electricity to the grid. The field of photovoltaic (PV) systems has garnered significant scholarly interest. For instance, in reference [52], the incremental conductance + integral regulator method was proposed as a means to train the maximum power point tracking (MPPT) controller. This method was designed to optimize the PV system's performance by ensuring that it operates at its maximum power point under varying solar irradiation conditions. Additionally, the study recommended the utilization of a Proportional–Integral (PI) controller for managing the DC–AC converter, which plays a crucial role in converting the direct current (DC) generated by the PV panels into alternating current (AC) for grid integration. However, it is noteworthy that these control methods exhibit instability when confronted with significant fluctuations in solar irradiation. The inherent variability in solar radiation, especially during periods of cloud cover or transitioning sunlight, poses a challenge to maintaining stable energy output. As solar irradiation decreases, there is an observed fluctuation in the amount of power injected into the grid. This phenomenon raises important considerations for the practical applications of PV systems, particularly those integrated into the power grid. While the controllers based on mathematical concepts have shown favorable results under relatively stable solar conditions, they may require further refinement to address the challenges posed by rapid and unpredictable variations in solar radiation. These findings emphasize the need for adaptive control strategies that can respond effectively to changing environmental conditions, ensuring grid stability and consistent energy supply. Future research in this area could focus on the development of advanced control algorithms that incorporate real-time weather forecasting or sensor-based feedback systems to enhance the robustness and adaptability of PV controllers. Additionally, exploring energy storage solutions, such as batteries, may provide a means to buffer the impact of solar irradiation fluctuations and further improve the reliability of grid-connected PV systems. Such advancements hold the potential to optimize the utilization of solar energy and contribute significantly to sustainable energy generation and grid integration.

4. Conclusions

In response to the urgent global imperatives surrounding the energy crisis, environmental sustainability, and the imperative to secure a viable future for generations to come, the integration of renewable energy sources stands out as an essential strategic endeavor.

Within the ambit of this research paper, an innovative photovoltaic (PV) system has been introduced, meticulously designed to incorporate predictive control methodologies while harnessing the inherent optimization capabilities of the Particle Swarm Optimization (PSO) technique. This synthesis of advanced approaches underscores the core objective: elevating the holistic performance and efficiency of PV systems, thus making a substantive contribution to a cleaner, more sustainable energy landscape. Through an exhaustive series of simulations meticulously executed on the MATLAB/SIMULINK platform, the research yielded highly promising results for the envisioned system. The implemented predictive control techniques exhibited commendable resilience, effectively maintaining a stable energy production profile in the face of dynamic fluctuations in solar radiation levels. Furthermore, the adaptability of the proposed system to rapidly changing weather conditions ensures a steadfast and dependable energy output, consolidating its status as a robust and resilient energy solution. As we cast our gaze toward the future, research endeavors in this domain will be judiciously directed toward the exploration and refinement of pioneering control methodologies custom-tailored for PV systems. The overarching aim is to further amplify the system's performance and efficacy, with an unwavering commitment to achieving even more remarkable and dependable results. In parallel, the research roadmap encompasses a comprehensive comparative analysis, a rigorous endeavor intended to systematically compare the effectiveness of these novel control methodologies with the performance metrics of the existing systems. This methodical approach promises to unveil the full potential of advanced control strategies, poised to shape the trajectory of renewable energy generation and seamless grid integration. In summation, this research advances the discourse on renewable energy by not only introducing an innovative PV system but also by demonstrating its inherent potential to address critical energy and environmental challenges. This contribution exemplifies the prospects of cutting-edge control methodologies and optimization techniques, setting the stage for a sustainable, greener, and more energy-efficient future.

Author Contributions: Conceptualization, C.B.; methodology, C.B.; software, C.B. and I.E.K.; validation, I.E.K. and B.B.; formal analysis, R.B., B.E.B., S.M. and A.Z.; investigation, C.B. and B.B.; resources, C.B. and R.B.; data curation, C.B. and I.E.K.; writing—original draft preparation, C.B, I.E.K. and B.B.; writing—review and editing, C.B, B.B., S.M., B.E.B. and A.Z.; visualization, B.B. and S.M.; supervision, I.E.K. and R.B.; project administration, R.B. and A.Z.; funding acquisition, B.B., S.M. and A.Z. All authors have read and agreed to the published version of the manuscript.

Funding: The research is partially funded by the Ministry of Science and Higher Education of the Russian Federation as part of the World-class Research Center program: Advanced Digital Technologies (contract No. 075-15-2022-312 dated 20 April 2022).

Data Availability Statement: Not applicable.

Conflicts of Interest: The authors declare no conflict of interest.

References

1. Ishaque, K.; Salam, Z. A review of maximum power point tracking techniques of PV system for uniform insolation and partial shading condition. *Renew. Sustain. Energy Rev.* **2013**, *19*, 475–488. [CrossRef]
2. Tolba, M.; Rezk, H.; Diab, A.A.Z.; Al-Dhaifallah, M. A Novel Robust Methodology Based Salp Swarm Algorithm for Allocation and Capacity of Renewable Distributed Generators on Distribution Grids. *Energies* **2018**, *11*, 2556. [CrossRef]
3. Tolba, M.A.; Rezk, H.; Tulsky, V.; Diab, A.A.Z.; Abdelaziz, A.Y.; Vanin, A. Impact of Optimum Allocation of Renewable Distributed Generations on Distribution Networks Based on Different Optimization Algorithms. *Energies* **2018**, *11*, 245. [CrossRef]
4. Cheng, Z.; Zhou, H.; Yang, H. Research on MPPT control of PV system based on PSO algorithm. In Proceedings of the 2010 Chinese Control and Decision Conference, Xuzhou, China, 26–28 May 2010; IEEE: Piscataway, NJ, USA, 2010; pp. 887–892.
5. Singh, G.K. Solar power generation by PV (photovoltaic) technology: A review. *Energy* **2013**, *53*, 1–13. [CrossRef]
6. Lun, S.; Du, C.; Sang, J.; Guo, T.; Wang, S.; Yang, G. An improved explicit I-V model of a solar cell based on symbolic function and manufacturer's datasheet. *Sol. Energy* **2014**, *110*, 603–614. [CrossRef]
7. Bai, J.; Liu, S.; Hao, Y.; Zhang, Z.; Jiang, M.; Zhang, Y. Development of a new compound method to extract the five parameters of PV modules. *Energy Convers. Manag.* **2014**, *79*, 294–303. [CrossRef]

8. Sun, B.; Yu, Y.; Qin, C. Should China focus on the distributed development of wind and solar photovoltaic power generation? A comparative study. *Appl. Energy* **2017**, *185*, 421–439. [CrossRef]
9. Ishaque, K.; Salam, Z.; Taheri, H. Simple, fast and accurate two-diode model for photovoltaic modules. *Sol. Energy Mater. Sol. Cells* **2011**, *95*, 586–594. [CrossRef]
10. Mellit, A.; Benghanem, M.; Kalogirou, S.A. Modeling and simulation of a stand-alone photovoltaic system using an adaptive artificial neural network: Proposition for a new sizing procedure. *Renew. Energy* **2007**, *32*, 285–313. [CrossRef]
11. Ahmed, A.S.; Berzoy, A.; Mohammed, O. Design and hard-ware implementation of FL-MPPT control of PV systems based on GA and small-signal analysis. *IEEE Trans. Sustain. Energy* **2017**, *8*, 279–290.
12. Vidhya, K.; Arfan, G.; Erping, Z. Modelling and simulation of maximum power point tracking algorithms and review of MPPT techniques for PV applications. In Proceedings of the 5th International Conference on Electronic Devices, Systems and Applications (ICEDSA), Ras Al Khaimah, United Arab Emirates, 6–8 December 2016; pp. 1–4.
13. Nandurkar, S.R.; Rajeev, M. Modeling simulation & design of photovoltaic array with MPPT control techniques. *Int. J. Appl. Power Eng.* **2014**, *3*, 41–50.
14. Babaa, S.E.; Armstrong, M.; Pickert, V. Overview of maximum power point tracking control methods for PV systems. *J. Power Energy Eng.* **2014**, *2*, 59–72. [CrossRef]
15. Faranda, R.; Leva, S. Energy comparison of MPPT techniques for PV systems. *WSEAS Trans. Power Syst.* **2008**, *3*, 446–455.
16. Kakosimos, P.E.; Kladas, A.G.; Manias, S.N. Fast Photovoltaic System Voltage- or Current-Oriented MPPT Employing a Predictive Digital Current-Controlled Converter. *IEEE Trans. Ind. Electron.* **2013**, *60*, 5673–5685. [CrossRef]
17. Esram, T.; Chapman, P.L. Comparison of photovoltaic array maximum power point tracking techniques. *IEEE Trans. Energy Convers.* **2007**, *22*, 439–449. [CrossRef]
18. Femia, N.; Petrone, G.; Spagnuolo, G.; Vitelli, M. Optimization of perturb and observe maximum power point tracking method. *IEEE Power Electron. Trans.* **2005**, *20*, 963–973. [CrossRef]
19. Kuo, Y.C.; Liang, T.J.; Chen, J.F. Novel maximum-power point tracking controller for photovoltaic energy conversion system. *IEEE Indust. Electron. Trans.* **2001**, *48*, 594–601.
20. El-Raouf, M.O.; Mosaad, M.I.; Al-Ahmar, M.A.; Bendary, F.M. MPPT of Hybrid solar-wind-grid power generation system. *Int. J. Ind. Electron. Drives-Inderscience Publ.* **2015**, *2*, 234–241.
21. Abed El-Raouf, M.O.; Mosaad, M.I.; Mallawany, A.; Al-Ahmar, M.A.; El Bendary, F.M. MPPT of PV-Wind-Fuel Cell of Off-Grid Hybrid System for a New Community. In Proceedings of the 2018 Twentieth International Middle East Power Systems Conference (MEPCON), Cairo, Egypt, 18–20 December 2018; pp. 480–487.
22. Barbosa, P.G.; Braga, H.A.C.; Rodrigues, M.C.B.; Teixeira, E.C. Boost current multilevel inverter and its application on single-phase grid connected photovoltaic systems. *IEEE Trans. Power Electron.* **2006**, *21*, 1116–1124. [CrossRef]
23. Kjaer, S.B.; Pedersen, J.K.; Blaabjerg, F. A review of single-phase grid-connected inverters for photovoltaic modules. *IEEE Trans. Industry Appl.* **2005**, *41*, 1292–1306. [CrossRef]
24. Calais, M.; Myrzik, J.; Spooner, T.; Agelidis, V.G. Inverters for single-phase grid connected photovoltaic systems—An overview. In Proceedings of the 2002 IEEE 33rd Annual IEEE Power Electronics Specialists Conference. Proceedings (Cat. No.02CH37289), Cairns, QLD, Australia, 23–27 June 2002; Volume 2, pp. 1995–2000.
25. Eltawil, M.A.; Zhao, Z. Grid-connected photovoltaic power systems: Technical and potential problems—A review. *Trans. Renew. Sustain. Energy Rev.* **2010**, *14*, 112–129. [CrossRef]
26. Kawabe, K.; Tanaka, K. Impact of dynamic behavior of photovoltaic power generation systems on short-term voltage stability. *IEEE Trans. Power Syst.* **2015**, *30*, 3416–3424. [CrossRef]
27. Ihedrane, Y.; Chakib, E.; Bossoufi, B. Direct and indirect field-oriented control of DFIG-generators for wind turbines variable-speed. In Proceedings of the IEEE 14th International Multi-Conference on Systems, Signals & Devices, Marrakech, Morocco, 28–31 March 2017; pp. 27–32.
28. Beriber, D. Optimization and Energy Management System of Production Wind-PV with Storage. Ph.D. Thesis, USTHB, Ezzouar, Algeria, 2010.
29. Parida, A.; Chatterjee, D. Cogeneration topology for wind energy conversion system using doubly-fed induction generator. *IET Power Electron.* **2016**, *9*, 1406–1415. [CrossRef]
30. Bakir, H.; Kulaksiz, A.A. Modelling and voltage control of the solar-wind hybrid micro-grid with optimized STATCOM using GA and BFA. *Eng. Sci. Technol. Int. J.* **2020**, *23*, 576–584. [CrossRef]
31. Rauschenbach, H.S. *Solar Cell Array Design Handbook*; Van Nostrand Reinhold: New York, NY, USA, 1980.
32. Barth, N.; Jovanovic, R.; Ahzi, S.; Khaleel, M.A. PV panel single and double diode models: Optimization of the parameters and temperature dependence. *Sol. Energy Mater. Sol. Cells* **2016**, *148*, 87–98. [CrossRef]
33. Nishioka, K.; Sakitani, N.; Uraoka, Y.; Fuyuki, T. Analysis of multicrystalline silicon solar cells by modified 3-diode equivalent circuit model taking leakage current through periphery into consideration. *Sol. Energy Mater. Sol. Cells* **2007**, *91*, 1222–1227. [CrossRef]
34. Patel, H.; Agarwal, V. MATLAB-based modeling to study the effects of partial shading on PV array characteristics. *IEEE Trans. Energy Convers.* **2008**, *23*, 302–310. [CrossRef]
35. El Hammoumi, A.; Motahhir, S.; Chalh, A.; El Ghzizal, A.; Derouich, A. Low-cost virtual instrumentation of PV panel characteristics using Excel and Arduino in comparison with traditional instrumentation. *Renew. Wind Water Sol.* **2018**, *5*, 3. [CrossRef]

36. Yıldıran, N.; Tacer, E. Identification of photovoltaic cell single diode discrete model parameters based on datasheet values. *Sol. Energy* **2016**, *127*, 175–183. [CrossRef]
37. Rhouma, M.B.; Gastli, A.; Ben Brahim, L.; Touati, F.; Benammar, M. A simple method for extracting the parameters of the PV cell single-diode model. *Renew. Energy* **2017**, *113*, 885–894. [CrossRef]
38. Chowdhury, S.; Chowdhury, S.P.; Taylor, G.A.; Song, Y.H. Mathematical Modeling and Performance Evaluation of a Stand-Alone Polycrystalline PV Plant with MPPT Facility. In Proceedings of the IEEE Power and Energy Society General Meeting—Conversion and Delivery of Electrical Energy in the 21st Century, Pittsburg, PA, USA, 20–24 July 2008.
39. Jung, J.-H.; Ahmed, S. Model Construction of Single Crystalline Photovoltaic Panels for Real-time Simulation. In Proceedings of the IEEE Energy Conversion Congress & Expo, Atlanta, GA, USA, 12–16 September 2010.
40. Nema, S.; Nema, R.K.; Agnihotri, G. Matlab/simulink based study of photovoltaic cells/modules/array and their experimental verification. *Int. J. Energy Environ.* **2010**, *1*, 487–500.
41. Haripriya, T.; Alivelu, M.; Rao, U.M. Performance evaluation of DC grid connected solar PV system for hybrid control of DC–DC boost converter. In Proceedings of the 10th International Conference on Intelligent Systems and Control (ISCO), Coimbatore, India, 7–8 January 2016; pp. 1–6.
42. Boubii, C.; El Kafazi, I.; Bannari, R.; El Bhiri, B. A Comparative Study Between MPC Algorithm and P&O and IncCond the Optimization Algorithms of MPPT Algorithms. In *Digital Technologies and Applications*; Motahhir, S., Bossoufi, B., Eds.; Springer Nature Switzerland: Cham, Switzerland, 2023; pp. 704–713.
43. Holtz, J.; Stadtfeld, S. A predictive controller for the stator current vector of AC machines fed from a switched voltage source. *Int. Power Electron. Conf. (IPEC)* **1983**, *1983*, 1665–1675.
44. Rodriguez, J.; Cortes, P. *Predictive Control of Power Converters and Electrical Drives*; John Wiley & Sons: Hoboken, NJ, USA, 2012; Volume 37.
45. Abu-Rub, H.; Guzinski, J.; Krzeminski, Z.; Toliyat, H.A. Predictive current control of voltage-source inverters. *IEEE Trans. Ind. Electron.* **2004**, *51*, 585–593. [CrossRef]
46. Soliman, M.; Malik, O.P.; Westwick, D.T. Multiple model multiple-input multiple-output predictive control for variable speed variable pitch wind energy conversion systems. *IET Renew. Power Gener.* **2011**, *5*, 124–136. [CrossRef]
47. Mohan, N.; Robbins, W.P.; Undeland, T.M.; Nilssen, R.; Mo, O. Simulation of power electronic and motion control systems-an overview. *Proc. IEEE* **1994**, *82*, 1287–1302. [CrossRef]
48. Adouairi, M.S.; Bossoufi, B.; Motahhir, S.; Saady, I. Application of fuzzy sliding mode control on a single-stage grid-connected PV system based on the voltage-oriented control strategy. *Results Eng.* **2023**, *17*, 100822. [CrossRef]
49. Oskouei, A.B.; Banaei, M.R.; Sabahi, M. Hybrid PV/wind system with quinary asymmetric inverter without increasing DC-link number. *Ain Shams Eng. J.* **2016**, *7*, 579–592. [CrossRef]
50. Saady, I.; Karim, M.; Bossoufi, B.; El Ouanjli, N.; Motahhir, S.; Majout, B. Optimization and control of photovoltaic water pumping system using kalman filter based MPPT and multilevel inverter fed DTC-IM. *Results Eng.* **2023**, *17*, 100829. [CrossRef]
51. Kafazi, I.E.; Bannari, R.; Boubii, C.; Bhiri, B.E.; Rafia, H. MPC-PSO of a DFIG and comparison with PI controller. In Proceedings of the 2023 5th Global Power, Energy and Communication Conference (GPECOM), Nevsehir, Türkiye, 14–16 June 2023; pp. 1–5. [CrossRef]
52. Saady, I.; Bossoufi, B.; Karim, M.; Motahhir, S.; Adouairi, M.S.; Majout, B.; Lamnadi, M.; Masud, M.; Jehad, F. Optimisation for a photovoltaic pumping system using indirect Field Oriented Control of Induction Motor. *Electronics* **2021**, *10*, 2670. [CrossRef]